JPhys Photonics

PAPER • OPEN ACCESS

Two-dimensional ultrafast transient absorption spectrograph covering deep-ultraviolet to visible spectral region optimized for biomolecules

Journal of Physics: Photonics

OPEN ACCESS

RECEIVED
9 March 2021

REVISED
26 April 2021

ACCEPTED FOR PUBLICATION
3 June 2021

PUBLISHED
21 June 2021

PAPER

Two-dimensional ultrafast transient absorption spectrograph covering deep-ultraviolet to visible spectral region optimized for biomolecules

Maryam Nazari Haghighi Pashaki, Nina Mosimann-Schönbächler, Aaron Riede, Michela Gazzetto, Ariana Rondi and Andrea Cannizzo*

Institute of Applied Physics, University of Bern, Sidlerstrasse 5, CH-3012 Bern, Switzerland
* Author to whom any correspondence should be addressed.

E-mail: andrea.cannizzo@iap.unibe.ch

Keywords: UV two-dimensional spectroscopy, ultrafast transient absorption spectroscopy, deep-UV time resolved spectroscopy, phenanthrene multichromophoric system, azurin

Supplementary material for this article is available online

Abstract

We report on the implementation of a multi-kHz single-shot referenced non-coherent two-dimensional UV spectrograph based on conventional pump-probe geometry. It has the capability to cover a broad spectral region in excitation from 270-to-380 nm and in the detection from 270-to-390 nm and 320-to-720 nm. Other setups features are: an unprecedented time resolution of 33 fs (standard deviation); signals are photometrically corrected; a single-shot noise of <1 mOD. It has the capability to operate with sample volumes as small as few μl which is an accomplishment in studying biological or biomimetic systems. To show its performances and potentials, we report two preliminary studies on the photophysics of phenanthrenes hosted in a multichromophoric antenna system and of aromatic amino acids in a blue-copper azurin.

1. Introduction

Transient absorption (TA) spectroscopy can provide precious information on the excited states dynamics of molecular systems, which are crucial to define the photocycle and to extract a model to rationalize the photophysics and photochemistry of the system under investigation. However, in the case of complex systems as biomolecules, supramolecular systems or polymers, conventional TA methods could not provide intelligible and conclusive insights because of overcrowded TA spectra difficult to interpret. An approach to overcome this limitation is multidimensional spectroscopy, which ultimately collect the optical response of the system as a function of detection and excitation wavelengths. It can provide information on the coupling between different chromophores and disentangle the homogeneous and the inhomogeneous contributions to the line shapes, helping to interpret overcrowded spectra. The heterodyne detected two-dimensional (2D) photon-echo spectroscopy is the most popular among all the multidimensional optical spectroscopy methods [1, 2]. It uses sequences of three resonant pulses, which are focused on the sample, usually in a non-collinear phase matching geometry, to generate a signal proportional to the 3rd order susceptibility $\chi^{(3)}$ [3, 4]. In this scheme the information is then extracted upon Fourier transformation of the spectrally resolved signal as a function of the time delay between the first and second pulses. Therefore, very broadband Fourier-limited excitation pulses can be used to achieve the shortest, Fourier limited time resolution without sacrificing spectral resolution. To extract the main information, mostly $\chi^{(3)}$, it is necessary to measure phase and amplitude of photon-echo signals emitted by the sample, by means of a heterodyne detection where the interferogram between the signal and a local oscillator field is measured. When it comes to investigate electronic transitions and couplings with sub-10 femtosecond (fs) resolution, Fourier-transform (FT) 2D spectroscopies are the techniques of choice.

However, this method needs several FT-limited and intense pulses with a spectrum broad enough to cover all the region of interest. In addition, these pulses must be phase-stable to an interferometric precision

($\Delta\phi < 2\pi/100$) [5]. This demanding task becomes formidable if the investigated spectral region is deep-UV, or DUV (the definition of DUV is in not univocal; in the following we will refer to the range 250–320 nm). Indeed, despite its widely use in the IR and the Vis [6–9], there are only few examples in the UV [1, 10, 11], and mainly limited to rather small excitation and probing ranges [1, 12, 13]. However, if the extreme time-resolution of few fs provided by an FT approach could be sacrificed, FT-2D techniques become an unnecessarily complex approach. In this case, the so called 2D transient absorption (2D TA) spectroscopy is much less demanding but still a very versatile and valid alternative [3, 10, 14]. This technique is an extension of the conventional TA scheme where the excitation dimension is added by implementing a tuneable narrowband excitation pulse, which can cover the relevant spectral region without the requiring phase-stability and simultaneous generation of all the spectral components. The main limitation of 2D TA methods with respect to FT-2D photon-echo is time resolution. Indeed, in the former, to keep the excitation selective, pump pulses are rather narrow ($\Delta\omega/\omega \sim 1\%$), corresponding to FT-limited lengths of 100 fs full width half maximum. Conversely a 2D photon-echo approach with FT-limited broadband pulses ($\Delta\omega/\omega \sim 10\%$–$20\%$) can potentially provide a time resolution of few tens of fs or less. This is highly desirable when pure electronic dynamics without involvement of nuclear motions are investigated. However, the vast majority of transfer processes in bio- and artificial macro-molecules are assisted, if not driven, by nuclear motion of the molecule itself and of the solvent. Spectral heterogeneity and inhomogeneous broadening are the optical counterparts of conformational distribution and dynamics of the molecule and of solvent fluctuations. For these reasons it is clear that similar to 2D photon-echo, 2D TA has still the potential to clarify these dynamics, vibrational and electronic coupling between molecules or chromophores, the presence of new relaxation channels and changes in their time scales or spectra. Such information can be crucial to understand and interpret ultrafast dynamics and photo-physical/-chemical events as, for instance, long-range energy or charge transfer processes.

Furthermore, extension of excitation and detection to DUV is an essential accomplishment. Indeed, exploiting UV chromophores to investigate structural and energy dynamics in biomolecules, has been one of the major drives to develop UV fs spectroscopies [2, 15]. This includes chromophores containing aromatic mono- or oligo-cyclic organic groups, for example aromatic amino acids, nucleotide bases, imides and (di-) imines. These species are constituents of bio molecules, many molecular devices and supra molecular structures. Exploiting them as a probe opens a new window on the dynamical properties of the macromolecule edifice in a site-specific fashion. They provide dynamical information on intramolecular electrostatics, fluctuations and local rigidity, structural changes, anharmonic coupling and long-range interactions as well as vibrational and electronic coherences [2, 15].

Another advantage of 2D-TA is that the probe pulse (the third pulse in a 2D photon-echo set-up) does not need to be intense and compressed as required in conventional FT schemes [1], which limits the detection range of FT 2D set-ups. Only recently with the advent of photonic quantum fibres this limitation has been partially removed [16, 17] but only within the Vis range. Conversely in a pump-probe scheme [2] probing uses a supercontinuum generated in bulk materials [18], which allows to cover the DUV to near-IR range simultaneously. With the aim to investigate functional dynamics in biological and bioinspired systems, the capability to cover simultaneously such an extended range is not just an add-value but a stringent requirement because: (a) several important cofactors as haem and flavo groups, retinals and metal containing proteins (e.g. copper proteins) have strong optical absorption both in the Vis and UV range; (b) the aforementioned UV chromophores, while they have the lowest transitions in the UV, exhibit excited state absorption (ESA) in the Vis. Therefore probing simultaneously from DUV to Vis (or even better to near-IR) allows to track down both the electronic dynamics at the cofactor and of the scaffold, identifying couplings and transfer processes among amino acids and the interplay between cofactors and amino acids. In metallo-macromolecules it allows to access intra-ligand transitions (typically in the DUV-UV) and metal–ligand or ligand–ligand transitions, which are often in the Vis region [19]. The possibility to monitor ground state bleach (GSB) recovery and the excited states dynamics of such chromophores, located in the UV and in the Vis, respectively, is an invaluable tool to identify dark intermediate states and to sketch the complete photocycle.

However performing a successful experiment on biomolecules, requires not only the choice of the suitable detection scheme but a smart blend of strategies to minimize photo-damages, to handle very small sample volumes, and to keep the signal-to-noise ratio (SNR) and acquisition rate high.

Here we implemented a 2D TA spectrograph with several methodological improvements including single-shot referenced detection, a broad excitation covering DUV to UV (270–380 nm) and detection range (270–750 nm), a time resolution of 33 fs standard deviation, an SNR of 10^5 per second of acquisition and the capability to work with sample volumes as small as few μl.

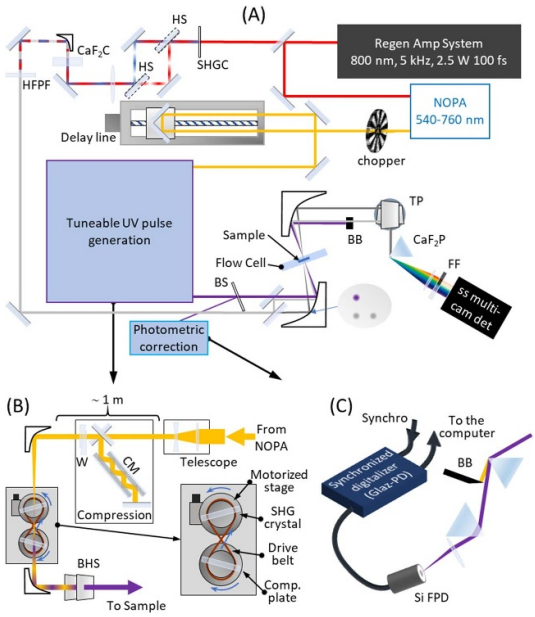

Figure 1. (A) Sketch of the 2D-UV spectrograph described in the main text. The tunable UV pulse generation stage and the photometric correction stage are shown in panel (B) and (C), respectively. A detail description is reported in the main text. Nomenclature: non collinear optical parametric amplifier (NOPA), second harmonic generation crystal (SHGC), harmonic separator (HS), CaF_2 crystal (CaF_2C), high frequency pass filter (HFPF), beam sampler (BS), beam blocker (BB), turned periscope (TP), CaF_2 prism (CaF_2P), flattening filter (FF); chirp mirrors (CM), UV grade wedges (W) broadband harmonic separators (BHS); Si fast photodetector (Si FPD).

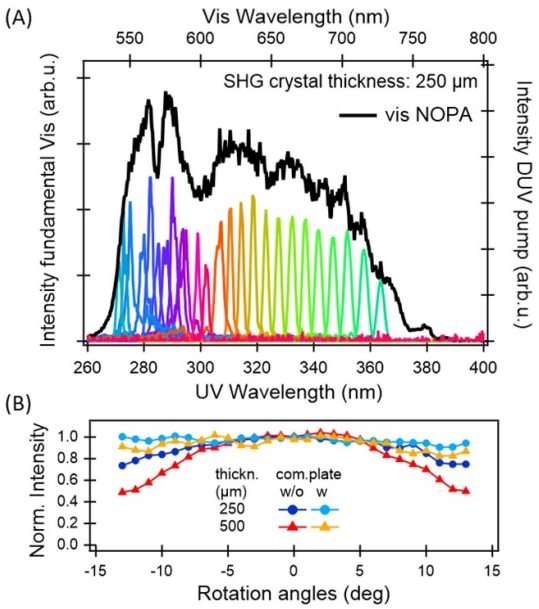

Figure 2. (A) An example of tuneable DUV pump pulses covering region from 270 nm to 370 nm generated with 250 mm β-BBO crystal. The typical spectral bandwidth is 1.8–2.4 nm. The fundamental broadband Vis source (black line) and pump wavelengths (coloured curves) are shown. (B) Beam walk-off versus rotation angle of the β-BBO, monitored as normalized intensity of the TA signal of rhodamine 800 dye detected at 581 nm (see figure S1) at 200 ps after excitation at 650 nm. The TA signals are normalized to the signal at 0°. The signal was measured using a 500 and 250 μm β-BBO crystal with and without a compensation plate.

2. Experimental setup

A scheme of the setup is shown in figure 1(A). About 90% of the output of a regenerative chirped pulse amplifier (5 kHz repetition rate, 500 μJ/pulse at 800 nm and pulse duration of 100 fs) is used to pump a commercial non-collinear optical amplifier (NOPA) by Light Conversion (Topas White). The NOPA was customized to generate ultra-broadband pulses with a spectrum from 520 to 760 nm (see figure 2(A)). The energy per pulse is typically 30 μJ, which gives an average spectral density of 100–150 nJ nm^{-1}.

The detection is based on a multi-camera detection platform, developed in our labs in collaboration with Synertronic Designs (Glaz by Synertronic Designs). It allows the implementation of a multi camera detection (up to eight cameras and photodetectors) with a readout rate up to 8 kHz and a single-shot SNR of 10^3 for spectra and 10^4 for pulse intensities. Its architecture is designed to collect the different signals without timing ambiguity.

We used two synchronized linear CMOS camera (Glaz PulseSync) and one photodetector (Glaz-PD equipped with a fast-biased silicon photodetector DET10A by Thorlabs) to collect simultaneously two spectra and the intensity of the pump pulse, shot-by-shot at 5 kHz. The noise on the acquired spectra is 14 μOD per second at 5 kHz. The advantage of a multi-camera single-shot detection will be discussed in section 2.3.

2.1. Pump beam generation and time resolution

As discussed in the introduction, DUV-to-UV 2D TA electronic spectroscopy collects TA spectra as a function of pump wavelength (λ_{Pm}) and therefore it needs a finely tuneable pump pulse in the DUV-to-UV region. For this purpose, we took inspiration from [14], where a broadband Vis source was frequency doubled by means of a rotating type I β barium borate (β-BBO) crystal. The rotation of the crystal allows to select the desired UV wavelength by phase-matching. The implementation reported in literature where based on a rather thick BBO crystals (2 mm) in favour of more second harmonic generation (SHG) efficiency and spectral resolution ($\Delta\lambda \sim 1.5$ nm) but at the cost of a dramatic beam walk-off (namely a parallel shift of the beam upon rotation of the crystal). Indeed, to cover the target UV range of 270–380 nm, the internal phase-matching angle of the β-BBO crystal should be rotated from 46.8° to 30.8°. Choosing a β-BBO crystal with an average cutting angle of 38.8° (the condition for doubling 620 nm), this corresponds to a rotation range of $\pm$13° for the external angle. With a 2 mm thick crystal this causes a walk-off of $\pm$170 μm (conversely the longitudinal shift is negligible, being less than 30 μm), which would cause a complete destruction of the pump/probe overlap at the sample position. Therefore, it is mandatory to compensate for the walk-off by sending UV beam through a counter-rotating BBO crystal with the same thickness. Despite a rather narrow bandwidth, the passage through 4 mm of bulk material, sets a limitation of hundreds of fs to the length of the tuneable UV pulses.

As it will be explained in the next section a key aspect of our strategy to friendly handle biomolecules is to use pump spots at the sample position with a diameter of few tens of microns. At this aim we carefully designed our SHG stage to minimize the distortions occurring at the β-BBO crystal.

The starting point was to reduce the crystal thickness compatibly with our desired spectral resolution. We observed that the expected bandwidth of a UV pulse at 300 nm, generated with a 2 mm thick β-BBO crystal should be ~0.3 nm and not 1.5 nm, since the expected Vis acceptance bandwidth is 40 cm^{-1} [20]. This confirms that most of the SHG occurs in the first 400 μm (0.3/1.5 $\times$ 2 mm) inside the crystal. As experimentally confirmed, we observed that a 500 μm thick crystal still generates UV pulses with a 1.2–1.5 nm bandwidth over all the range of interest but with a walk-off of only $\pm$40 μm.

To minimize this residual walk-off and to optimize the SHG efficiency we conceived the tuneable SHG scheme depicted in figure 1(B). It consists of a telescope to control the spot size at the SHG crystal, a compression stage to optimize the pulse duration and SHG efficiency of the UV pulses, and a motorized rotational stage for the SHG β-BBO. The rotational stage is mechanically connected with a twisted drive belt to another rotational stage. This allows to add optionally a counter rotating plate to compensate for the beam walk-off.

The Vis pulse is focused inside the SHG crystal and the telescope, which is placed 1 m far from the focusing parabolic mirror, is used to control the size of the beam waist. This is achieved by finely changing the distance between the telescope lenses (a planoconcave with $f = -50$ mm and a planoconvex with $f = 150$ mm). The advantage of this assembly is twofold. First it allows to choose a waist beam size much larger that the walk-off displacement. Therefore, the pump spot on the sample which is an image of the spot on the SHG crystal will not move significantly. Second, we can optimize the Vis beam fluence to reach the highest SHG efficiency before other undesired processes (mainly white light generation and photodamage of the SHG crystal) are induced. The optimal waist size was 150 μm which allows us to achieve 20–30 nJ excitation energy at the sample position (sufficient to excite bio- and bio-mimetic samples).

The rotation of the SHG crystal was controlled with a motorized continuous rotational stage (CR1-Z7 by Thorlabs) based on an incremental encoder with the precision of 2.19 arcsec and the maximum speed of 6° s^{-1}.

Figure 2(A) shows representative UV pump spectra obtained by SHG of fundamental Vis using this method. The different UV spectra are generated at different phase matching angle of 250 μm β-BBO crystal and are calibrated versus the angles, using a commercial UV–Vis spectrometer (Shamrock-500i spectrograph by Andor).

To quantify the effect of the beam walk-off on the pump-probe signal, we measured the amplitude of a TA signal of a long-lived visible dye at a fixed delay after the excitation (specifically, Rhodamine 800 in ethanol upon 650 nm excitation at 200 ps) as a function of the rotation angle of the β-BBO (figure 2(B)). We chose a visible dye to keep the excitation wavelength fixed regardless of the β-BBO angle. Also, we measured the TA at a long delay to neglect the effect of the rotation on the time-zero. Since at the phase-matched condition the refraction index of the Vis and UV lights are the same, the observed plots are valid also upon UV excitation. We tested different crystal thickness with and without the compensation plate. We observed that the effect of the rotation with the 500 μm crystal is acceptable within $\pm$10% for rotations of $\pm$10°. This corresponds for instance to a range of 280–360 nm or, with a crystal cut at 36.4° (phase-matching for 650 nm) to a range of 290–385 nm. Such ranges are enough for most of the spectroscopic applications. If a full UV range of 270–380 nm must be covered, the effect can be compensated in post analysis or by adding a compensation plate on the counter-rotating mount. In the latter case we used as a compensation plate another β-BBO crystal with the same thickness. To prevent higher harmonic generation the ordinary axis was set perpendicular to the one of first β-BBO crystal. Alternatively, we also tested a 250 μm thick β-BBO crystal which practically made the use of compensation plate unnecessary even for the widest rotation range (according to a walk-off of only $\pm$20 μm). However, this is at the cost of less spectral resolution and UV pulse energy.

Regarding the compression strategy, we tested a prism-based compressor and a pair of chirped mirrors (by Layertec) with UV grade wedges for fine compensation. The former is more cost effective, but its capability to compensate the pulse chirp over a so wide spectrum is unsatisfactory. Therefore, the compression can be optimized to have SHG around the optical absorption of the investigated system, but the energy spectral density drops at further wavelengths. We used highly dispersive SF11 prisms to save room on the table and avoid very long synchronization lines, but better performance could be obtained with UV-grade prisms. Conversely the use of chirp-mirrors to control the pulse compression is definitively a better choice. It allows indeed to compress the ultrabroad NOPA pulse, and to add finely a linear over-compression in combination with UV-grade wedges. The latter is crucial to control undesired nonlinear effects and to achieve the best length at the sample position of the UV pulses.

The UV and Vis radiation are separated with broadband shallow angle harmonic separators by Light Conversion, which achieve more than 90% UV reflection in the region 270–350 nm and 345–420 nm.

The UV pump is recollimated by a parabolic mirror ($f = 150$ mm) after the SHG β-BBO and then focused on the sample by another parabolic mirror ($f = 120$ mm). The pump spot size at sample position is approximately 60 μm diameter ($1/e^2$) and it is blocked after sample. A special care was taken to ensure that the pump and probe beams are parallel to each other and to the axis of the parabolic mirror. In this way the overlap at the sample position is automatically achieved (the Rayleigh length is 9 mm) and any effect due to parallel shift of the pump beam, when the delay line is moved, is minimized.

To estimate the time resolution, we measured cross-correlation between the pump and the probe pulses in a 150 μm sapphire plate at the sample position (data not shown). We measured an unprecedented temporal resolution of 33 fs (standard deviation) using the 250 μm β-BBO crystal without compensation plate and 45 fs using the 500 μm β-BBO crystal with compensation plate. Accordingly, the main limitation to investigate sub-100 fs transients is only the contamination of the cross-phase modulation (CPM), when it is comparable with or stronger than the TA signals.

2.2. Probe and reference pulses generation and detection

To generate white light in the region 320–720 nm, $\sim$1 μJ of 800 nm light is focused into a 5 mm thick CaF_2, which is continuously wobbled to avoid damage due to accumulated heat. To shift the supercontinuum spectra towards the DUV region, the CaF_2 crystal is pumped with 400 nm pulse, by frequency doubling of the fundamental (see figure 1). The 400 nm radiation is filtered out by a UV fs dielectric mirror (by Eksma Optics) with high reflectivity at 400 nm (>99%) and high transmission at 240–370 nm (>70%–90%, depending on the wavelength). The resulted spectrum at the sample position is shown in figure 3, which covers from 270 to 390 nm. The loss at $\lambda < 270$ nm is due to less reflectivity of the broadband UV-enhanced aluminium mirrors steering the probe beam through the sample.

Afterward, the supercontinuum is collimated and then split by a 50/50 UV–Vis beam-splitter. One of the two beams is used as a probe and focused to spatially overlap with pump in the sample. The delay time between pump and probe is controlled by a motorized delay stage placed in pump path. The probe replica passes through an unexcited sample region and is used as reference spectrum. Both reference and probe are recollimated by another parabolic mirror ($f = 120$ mm) and then are spectrally dispersed by a CaF_2 prism on the two liner detectors.

We opted for a prism as a dispersive element instead of a grating, because: (a) only prisms can provide constant and unitary transmission over all the detection range (270–750 nm), on condition to be at the

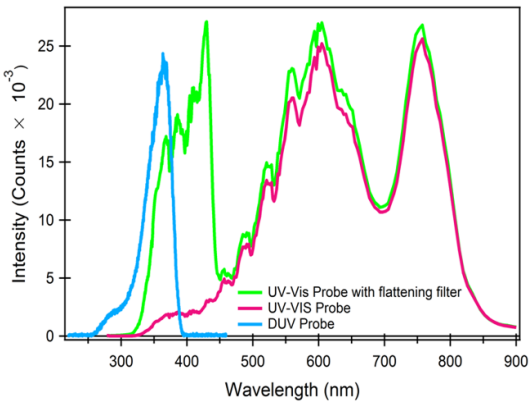

Figure 3. DUV and UV–Vis continuum used for probing. The UV–Vis spectrum after the flattening filter is also shown.

Brewster angle at the central wavelength; (b) it allows us to cover more than one octave since there is no spectral ambiguity due to the presence of λ and 2λ in the probe spectrum; (c) it provides a better spectral resolution at shorter wavelengths ($\Delta\lambda = 0.1$ nm at 280 nm; 1 nm at 600 nm and 10 nm at 800 nm) which is, as discussed in the introduction, an added value to investigate biomolecules.

To achieve the best spectral resolution the dispersed beams are collimate with a 4 f scheme consisting of a cylindrical lens ($f = 150$ mm for UV–Vis and $f = 100$ mm for DUV-UV). Since the beam diameter is typically 1–2 mm but the vertical size of the pixels is 500 μm, in order to improve light collection, two short-focus cylindrical lenses ($f = 20$ mm) are placed in front of the camera to vertically focus each wavelength of the probe and reference on each pixel. This enhances the statistical noise by a factor of 2–4 at shorter wavelengths, where we are always in a statistical regime because we cannot compensate a limited number of counts by increasing the probe and reference intensity).

To increase at maximum the SNR in the UV range, we use a flattening filter to selectively reduce the amplitude of the Vis part of the probe and reference spectra. Indeed, in the case of UV–Vis probing, the peak intensity of the continuum is strong enough to saturate the detection (figure 3). Instead of attenuating uniformly the probe intensity, which would result to the detriment of signal statistics in the UV tail, we use a custom made metallic neutral density filter by Altechna UAB, where half has 1.0 OD and the other half is transparent. To avoid artefacts due to multiple reflections; the side facing the detector is treated with a UV–Vis anti-reflection coating. By inserting it in front of the detector, the probe intensity at $\lambda > 400$ nm is attenuated by a factor 10, whereas the shorter wavelengths are not affected.

2.3. Signal calculation and photometric correction

To minimize the acquisition time, we implement a referenced detection where probe spectra are shot by shot acquired individually and are corrected, before averaging, for background and offsets, spectral and amplitude fluctuations of the white light and for instantaneous pump intensity.

As we will show in details when discussing the scientific cases, a unique advantage of 2D spectroscopy with respect to more conventional one-dimensional (1D) techniques, is the feasibility to extract time resolved signals at a given probe wavelength (λ_{pr}) as a function of the excitation wavelength (TA vs excitation, or TAE, spectra) at different time delays. However, to collect meaningful action spectra, they need to be corrected for the power spectrum of the excitation (photometric correction). In this way, the TA signal should be proportional to the absorption spectrum, namely the percentage of excited molecules. At this purpose, a 150 μm thick uncoated window is inserted in the pump path to act as a beam-sampler. The picked-up beam is sent to a photodetector and used to correct for changes in the pump intensity. They include the dependency on the λ_{Pm} but also shot-to-shot fluctuations and drifts. To perform a proper photometric correction, it is mandatory to avoid any residual Vis light on the photodetector and beam steering movements. This is achieved (figure 1(C)) by dispersing and recollimating the sampling beam with a pair of UV fused-silica prisms set at the Brewster angle for the central wavelength of the UV component, and then by focusing it on the active area of the photodetector. Most of the Vis contamination, being S polarized, is filtered out by the prisms since it is not at the Brewster condition. The remaining Vis scattering is blocked by a beam block. With this assembly the Vis scattering on the photodetector is not detectable and the signal is only proportional to the UV pump intensity and insensitive to beam pointing instabilities.

Applying all these corrections, the single-shot TA signals ($\mathrm{TA}_i(\lambda_{\mathrm{pr}})$) at a given time delay and as a function of λ_{pr} (for the sake of readability the dependence on t is omitted), is calculated as:

$$\mathrm{TA}_i(\lambda_{\mathrm{pr}}) = \frac{-2}{\ln(10)}\left(\frac{p_0}{p_i}\right)\frac{\frac{I_{\mathrm{p}}(\lambda_{pr})_i}{R_{\mathrm{p}}(\lambda_{\mathrm{pr}})_i} - \frac{I_{\mathrm{u}}(\lambda_{\mathrm{pr}})_i}{R_{\mathrm{u}}(\lambda_{\mathrm{pr}})_i}}{\frac{I_{\mathrm{p}}(\lambda_{\mathrm{pr}})_i}{R_{\mathrm{p}}(\lambda_{\mathrm{pr}})_i} + \frac{I_{\mathrm{u}}(\lambda_{\mathrm{pr}})_i}{R_{\mathrm{u}}(\lambda_{\mathrm{pr}})_i}} \tag{1}$$

where $I_{\mathrm{p/u}}(\lambda_{\mathrm{pr}})_i$ and $R_{\mathrm{p/u}}(\lambda_{\mathrm{pr}})_i$ are two consecutive pumped (p) and unpumped (u) probe and reference spectra, respectively, corresponding to the pump pulse i, and corrected for the room light and detector offset. The consecutive unpumped and pumped spectra are obtained using a chopper in the pump beamline at 2.5 kHz.

The photometric correction is accounted for by the factor p_0/p_i, where p_0 and p_i are the shot-to-shot pump intensity recorded at the beginning of the experiment and corresponding to the pump pulse i, respectively.

To decrease the statistical noise and achieve a better SNR we average the signal over several shots (typically 2500 shots or equivalently 1 s per delay point):

$$\mathrm{TA}(\lambda_{\mathrm{pr}}) = \frac{1}{n}\sum_{i=1}^{n}\mathrm{TA}_i(\lambda_{\mathrm{pr}}). \tag{2}$$

2.4. Sample handling

A special care was devoted to sample handling. Photo damages due to multiple excitations and photo accumulation is a general issue with fs pulses, which is even more critical with biomolecules and molecules with the low-lying allowed transition in UV. Part of our strategy was to adopt a detection system with high SNR to reduce the acquisition time and the pump intensity. Indeed, as previously discussed in section 2.2, and proven in the last part of the article, we can detect TA spectra with amplitudes as small as tens of μOD upon excitation with 10 nJ pulses in less than one second. However, this can only partially mitigate such risks and often the only solution is to work in a single-shot-per-spot excitation regime. In this regime the photo excited sample volume is completely refreshed between one excitation and the next to avoid multiple excitations that, with UV photons, could easily ionize the molecule or cleave a bond. Considering that typical excitation conditions are: a pump spot of 150–200 μm diameter; a flow-cell with section area of 1–2 mm^2 and a 1–10 kHz repetition rate, this regime is achieved with a flow speed of 1–2 cm^3 s^{-1} or $\sim$0.1 l min^{-1}.

So far to achieve such values two solutions are commonly used: a flow-cell connected with a gear pump or a spinning cell [21]. The former needs several ml of solution because of the dead volume of the gear pump heads and of the tubing and mostly to allow bubbles to leave the solution. However, except very few exceptions such as commercially available myoglobins or cytochromes, the typical amount of sample in case of biomolecules is very small and the total volume to handle is $\lesssim 100\,\mu$l. In addition, biomolecules could suffer by the mechanical stress and the increased temperature induced by the fast-rotating micro-gears inside the pump head. Spinning cells need less amount of sample but still several hundreds of μl (typ. $\sim$0.5 ml) and their fast rotation induces high levels of mechanical and optical noise [21]. This substantially extends the length of the acquisition putting a strain on the photo and thermal stability of the sample.

After the improvements of fs technology in the last decades in terms of stability, repletion rates, tuneable sources, high-SNR and fast acquisition, a suitable sample handling, able to flow solutions without mechanical noise and dead volume, is probably the remaining main limitation to an extensive use of fs spectroscopy techniques to investigate biological systems.

To remove this obstacle, we conceive an original microfluidic scheme where, instead of circulating the solution, a step-motor syringe pen, synchronized with the laser frequency, is used to move the solution back and forth through a 1 mm $\times$ 0.2 mm quartz capillary with polish surfaces (figure 4). Since the pump spot on the sample is 60 μm, the single shot regime is achieved by delivering a single dose of 12 nl per shot with a rate of 5 kHz. We chose a pen-type syringe pump with micro-step motor (SBP series by Takasago) with a volume of 100 μl, a dose delivery resolution of 0.2 nl and an operational speed of up to 30 kHz. This system allows us to reach the optimal single-shot regime because the volume is shifted exactly by the spot size and at the laser repetition rate. The syringe can also be synchronized with the pump and probe shutters to avoid photo-accumulation at the turning points. The capillary is a customized quartz glass flow cell (by Starna Scientific Ltd) with a 20 mm $\times$ 1 mm $\times$ 0.2 mm micro channel connected with flexible PTFE tubing with an internal diameter of 200 μm. The walls of the flow cell are optically polished and with a thin aperture window of 200 μm at the detection area to minimize the group velocity dispersion (GVD) of the pump and probe pulses.

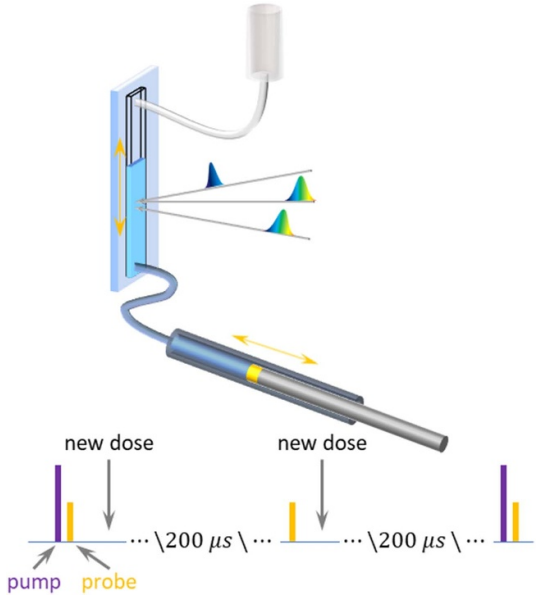

Figure 4. (Top) Implemented design using step-motor syringe pump and a microfluidic flow cell (see text for details). (Bottom) Timing chart showing the sequence of pump, probe and sample refreshing.

About the smallest sample volume useable, we should consider that 1 μl inside the microchannel is 5 mm height and corresponds to 83 doses of 12 nl each. Thanks to the surface tension inside the capillary the solution can be trapped in the middle and be moved up and down by inverting the flow direction each 16 ms (=83/5000 s). Such a switching rate is feasible with our syringe pump but at its limit. Therefore for long-lasting experiments it would be more recommended to use fast switching pumps, as piezoelectric membrane pumps, however the general approach would be the same. That is to say that potentially the volume can be as small as few μl and the main limitation is practically the maximum number of excitation cycles of the investigated system.

We carried out experiments with such small volumes but for most of our experiments, as the scientific cases discussed in the following, we use 30–50 μl which give a switching rate of 0.5–0.8 s.

2.5. Data collection and analysis

To collect 2D TA data we measured photometrically corrected TA signals as a function of λ_{Pm} for each delay time t. The collected data is a three-dimensional (3D) matrix $\mathrm{TA_{2D}}\left(\lambda_{\mathrm{pm}}, \lambda_{\mathrm{pr}}, t\right)$.

Nowadays, to extract the essential information from spectro-temporal data, advanced global data analysis techniques are routinely used. Several strategies are available as global lifetime and target analysis or lifetime distribution analysis [22, 23]. However, regardless the specific method, they are all conceived to decompose data on two dimensions, namely time and probe wavelength. For instance, the most popular method, based on singular value decomposition (SVD), aims to describe the experimental data, $\mathrm{TA_{1D}}\left(\lambda_{\mathrm{pr}}, t\right)$ in terms of a reduced number, P, of decay associated spectra ($\mathrm{DAS}\left(\lambda_{\mathrm{pr}}\right)$) and corresponding time constants, τ [24, 25]:

$$\mathrm{TA_{1D}}\left(\lambda_{\mathrm{pr}}, t\right) = \sum_{i=1}^{P} \mathrm{DAS}_i\left(\lambda_{\mathrm{pr}}\right)\left[\mathrm{e}^{\frac{t}{\tau_i}} \cdot u\left(t\right) \otimes f_{\mathrm{IRT}}\right] = \sum_{i=1}^{P} \mathrm{DAS}_i\left(\lambda_{\mathrm{pr}}\right) {\mathrm{e}_{\mathrm{IRF}}}^{-t/\tau_i} \tag{3}$$

where ${\mathrm{e}_{\mathrm{IRF}}}^{-t/\tau_i}$ represents an exponential decay with decay constant τ_{i} multiplied by a Heaviside step function, $u\left(t\right)$, and then convoluted with the instrumental response function, f_{IRT}. This is usually supposed Gaussian to allow calculating analytically the convolution operator $\otimes$. The extension of this method to 3D data $\mathrm{TA_{2D}}\left(\lambda_{\mathrm{pm}}, \lambda_{\mathrm{pr}}, t\right)$ would allow to describe them in terms of decay associated 2D spectra, $\mathrm{DA2DS}\left(\lambda_{\mathrm{pm}}, \lambda_{\mathrm{pr}}\right)$:

$$\mathrm{TA_{2D}}\left(\lambda_{\mathrm{pm}}, \lambda_{\mathrm{pr}}, t\right) = \sum_{i=1}^{P} \mathrm{DA2DS}_i\left(\lambda_{\mathrm{pm}}, \lambda_{\mathrm{pr}}\right) {\mathrm{e}_{\mathrm{IRF}}}^{-t/\tau_i}. \tag{4}$$

DA2DSs can give valuable information on the interactions between different transitions frequencies and their characteristic times.

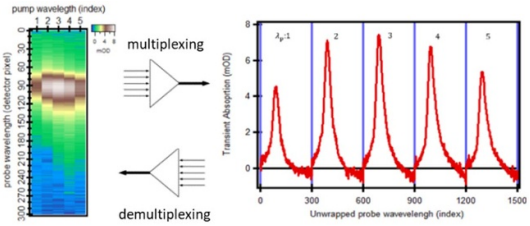

Figure 5. Conversion of a 2D matrix, representing a 2D spectrum at a given time, into a 1D vector upon multiplexing and vice versa (demultiplexing).

At this aim we multiplexed the 3D matrix into a 2D matrix by combining each 2D spectrum at a given time into a 1D spectral vector TA_{1D} (λ_j,t), where the probe spectrum of the first λ_{Pm} occupies the first N_{pr} (number of probe points), the second probe spectrum occupies the second N_{pr} points, and so on (see figure 5, and figures S2 and S3 (available online at stacks.iop.org/JPPHOTON/3/034014/mmedia)). $TA_{1D}\left(\lambda_j,t\right)$ is a sequence of 1D TA sub matrices $(N_{pr} \times t)$ for each excitation wavelength, where λ_j runs over all the $(\lambda_{Pm},\lambda_{Pr})$ pairs and $j = (1, \ldots, N_{pm} \times N_{pr})$.

Before carrying out the global analysis, it is still necessary to correct for the GVD of the probe continuum and the different arrival times of each pump pulse. This is due to changes in the pump optical path upon rotation of the SHG crystal and, if used, of the compensation plate, as well as uncompressed GVD of the Vis NOPA signal. The former is independent of λ_{Pm} and the same for each 1D TA sub matrix. The latter is achieved by measuring the delay of the signal rise at a given probe wavelength for all the λ_{Pm} (figure S3). After the removal of noisy spectral regions (mainly due to lack of probe light and CPM), the so-prepared data at this stage are ready to be analysed with the SVD global analysis for 2D spectro-temporal data previously illustrated. The obtained 1D DASs are finally converted into DA2DSs by demultiplexing (figure 5). A detailed example of the analysis of the azurin data is reported in supplementary information (figures S2 and S3).

In conclusion of this section it is worth noticing that the herein discussed strategy to multiplex 3D signals to use analysis tools conceived for 2D matrixes is valid for any other available method and is not limited to SVD approach only.

3. Scientific cases

To show the capability of our setup to measure 2D spectra in the DUV region on biological samples and the analysis method, we will present in the following two preliminary studies on a bio-inspired multichromophore antenna made by stacked phenanthrenes and on an electron transfer Cu protein (a *Pseudomonas aeruginosa* azurin) [26, 27].

The former represents an example of how this technique can easily provide rich information on the dynamical and static aspect of conformational and spectral heterogeneity in a supramolecular system. With the latter we will show the capability of UV 2D spectroscopy on biological systems to investigate couplings between different aromatic amino acids (in this case one tryptophan and three tyrosines).

3.1. DNA hosted multi chromophoric system

Here we report the preliminary study of energy transfer (EnT) in a DNA-guided multichromophoric system (MCS) previously reported in literature [28, 29]. In these systems, DNA is used as a framework for the generation of ordered assemblies of π-stacked arrays of phenanthrene and pyrene building blocks (figure 6(A)). They show a very efficient long-range EnT, which relies on a strong π-stacking interaction between the chromophores [28, 30–32] which allows the formation of highly delocalized excited states. Self-assembling MCS made by phenanthrenes has shown an impressive EnT distance over 150 nm) [33]. Studying these systems by means of 2D UV spectroscopy aims to unwrap the manifold of optical transitions of such multichromophoric structure, to characterize the coupling between different incorporated chromophores present in the MCS, and to track down homogeneous and inhomogeneous relaxation pathways. Figure 6 shows a selection of 2D spectra at different time delays after photo excitation of the MCS in water.

This comparison shows a clear dependence of the ESA on λ_{Pm}. In sub-ps dynamics we observe a change in the shape of the 2D spectra from an elliptical to a rounder shape, revealing a spectral diffusion [3]. This is better visualized by plotting the average spectral position (red dots in figures 6 and 7) as a function of λ_{pr} at

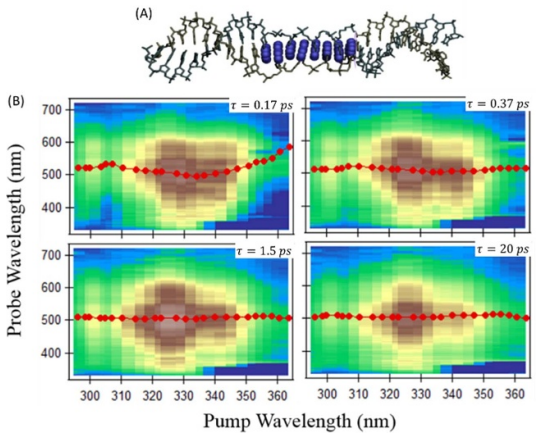

Figure 6. (A) A drawing of the investigated DNA-hosted MCS of staked phenanthrenes (blue shaded units). A representative selection of 2D spectra of the MCS in water at different times (0.17, 0.37, 1.5, 20 ps). Average spectral position, calculated according to equation (5) for each excitation wavelength are shown by red markers.

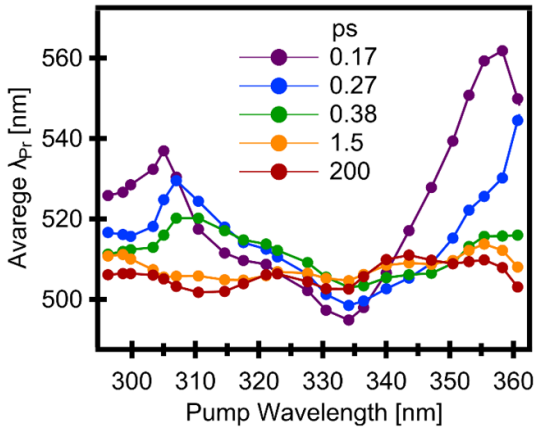

Figure 7. Average spectral position calculated according to equation (5) from figure 6 at different delay times.

different time, t, namely:

$$\lambda_{\mathrm{pr}}\left(\lambda_{\mathrm{Pm}}, t\right) = \frac{\int \lambda_{\mathrm{pr}} \mathrm{TA}_{\mathrm{2D}}\left(\lambda_{\mathrm{Pm}}, \lambda_{\mathrm{pr}}, t\right) \mathrm{d}\lambda_{\mathrm{pr}}}{\int \mathrm{TA}_{\mathrm{2D}}\left(\lambda_{\mathrm{Pm}}, \lambda_{\mathrm{pr}}, t\right) \mathrm{d}\lambda_{\mathrm{pr}}}. \tag{5}$$

This analysis also shows a similar behaviour in the region $\lambda > 340$ nm but with the opposite slope. Even without a detailed microscopic model, this evolution from a strong dependency on the pump wavelength to an almost constant behaviour, is a clear signature of a transition from an inhomogeneous to a homogeneous spectral response. The decay of spectral heterogeneity could originate from a decreased conformational disorder of the system, which is more flexible and softer in the ground state, whereas it becomes stiffer in the excited state. Alternatively, it could indicate that the equilibrated excited state is less sensitive to conformational disorder than the freshly excited ones. In both cases, these are evidences that reveal a great extent of conformational disorder of the ground state that reflects in an initial heterogeneity of the electronic excited states. This heterogeneity, regardless of electronic or conformational origin, disappears in few ps.

It is worth noticing that the presence of three distinct λ_{Pm} ranges with different behaviours (296–305 nm, 305–335 nm, 335–360) could be explained as a manifestation of conformational heterogeneity along with a non-monotonic mapping between conformational and optical variables. Alternatively, it could be rationalized as the initial presence of three different higher excited states which relax to the lowest excited one in sub-ps. As a general remark, it is always difficult to discriminate between the two descriptions without a microscopic model and computational simulations. However, the presence of a clear dependency on λ_{Pm} in each range (figure 7), which is smooth and continuous over each range and that uniformly decays to a constant value, and the debateable assumption of a sub-ps internal conversion (typically of few tens of fs)

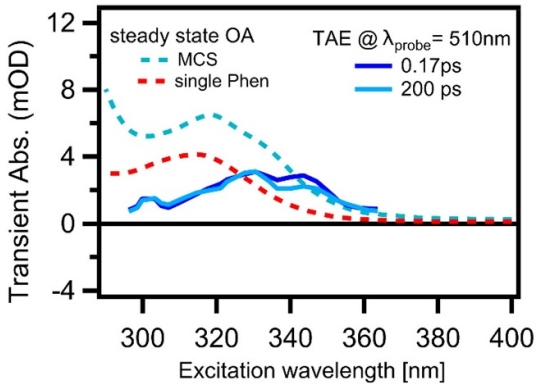

Figure 8. Comparison of the TA excitation (TAE) spectrum at $\lambda_{pr} = 510$ nm at the delay time t = 0.37 ps and 200 ps with the steady state electronic absorption spectrum (OA) of the MCS (figure 6(A)).

make spectral diffusion as the most reasonable explanation for the observed evolution. That said, clarifying the origin of the heterogeneity and the nature of the sub-ps dynamics needs further investigation also to identify the possible presence of short-lived intermediate states.

Another unique advantage of 2D spectroscopy is the possibility to extract TAE spectra at a given probe wavelength and time delay. Such plots are impossible with conventional 1D techniques and immediately reveal which transitions contribute more to the optical response of the system at a given wavelength and at a specific/relevant time. This makes 2D spectroscopy a superior spectroscopic tool able to disentangle the manifold of optical transitions underneath an apparently homogenous steady state optical absorption band. Figure 8 compares the steady-state absorption spectra with photometric TAE spectra at early and late time delays (0.37 ps and 200 ps) and $\lambda_{Pr} = 510$ nm, where the maximum of the signal is observed. The comparison shows that the TAE spectra are totally different from the stationary absorption spectrum revealing that the latter is actually due to a manifold of transitions, which can give origin to different dynamical behaviours of the MCSs. In particular the region 300–320 nm is dominated by transitions to excited states that preferentially relax back to ground state, and therefore not contributing to the population of the phenanthrenes in the MCS. Since the maximum of excited state population is observed in the region 320–340 nm, the transitions responsible of the MCS photophysics are red shifted with respect to the isolated phenanthrenes (red dashed curve in figure 8), contrary to what the steady state absorption of spectrum of the MCS would suggest. It shows two peaks at 320 nm and at 335 nm and the comparison with the TAE spectra allows to assign them to different electronic states, ruling out for instance the hypothesis that they are two vibronic replicas of the same electronic transition. All this information is crucial for a consistent microscopic modelling of ultrafast energy relaxation and transfer dynamics in such MCSs and a more extensive study is underway.

3.2. Pseudomonas aeruginosa azurin

In this blue copper protein a long-range electron transfer from the surface to the acceptor (a Cu^{II} ion) is mediated by a tryptophan (Trp) inside the protein, which contains also three tyrosines (Tyr) [26]. The former amino acid absorbs at 300–270 nm, whereas the Tyr steady state absorption is located at 250–290 nm [34, 35] (figures 9(C) or (D)). Therefore, the fact that overall absorption band in figure 9(C) is due to a manifold of transitions of different origin is out of question but it is a key point to disentangle their contributions to the protein photophysics. Tracking down the couplings between the Trp and the Tyrs in the protein is no less important to correctly model the energy and electron transfer processes in such systems [26, 35]. For this purpose, we performed a 2D-UV study spanning the pump wavelength over the steady state absorption region of these amino acids, namely 300–270 nm.

For the purposes of article, this section will give an example of the DUV detection and of the 3D SVD global analysis. Indeed, we exploited our capability to probe in the DUV region (270–370 nm), where the ground state transitions and the corresponding emissions are centred (figure 9(C)). This opens a window on the dependency of the relaxation channels and conformational heterogeneity (monitored via the recovery of GSB and via spectral heterogeneity of the emission signal, respectively) on the excitation wavelength.

Figure 9 shows a representative selection of 2D spectra of a wild-type *P. aeruginosa* azurin at physiological conditions at different times (0.12, 0.25, 1.25, 50, 200 ps). The experimental data are analysed with the 3D SVD-GA method discussed in section 2.5 and data are well described by 4 DA2DSs, which are shown in figure 9(B) with the respective characteristic times.

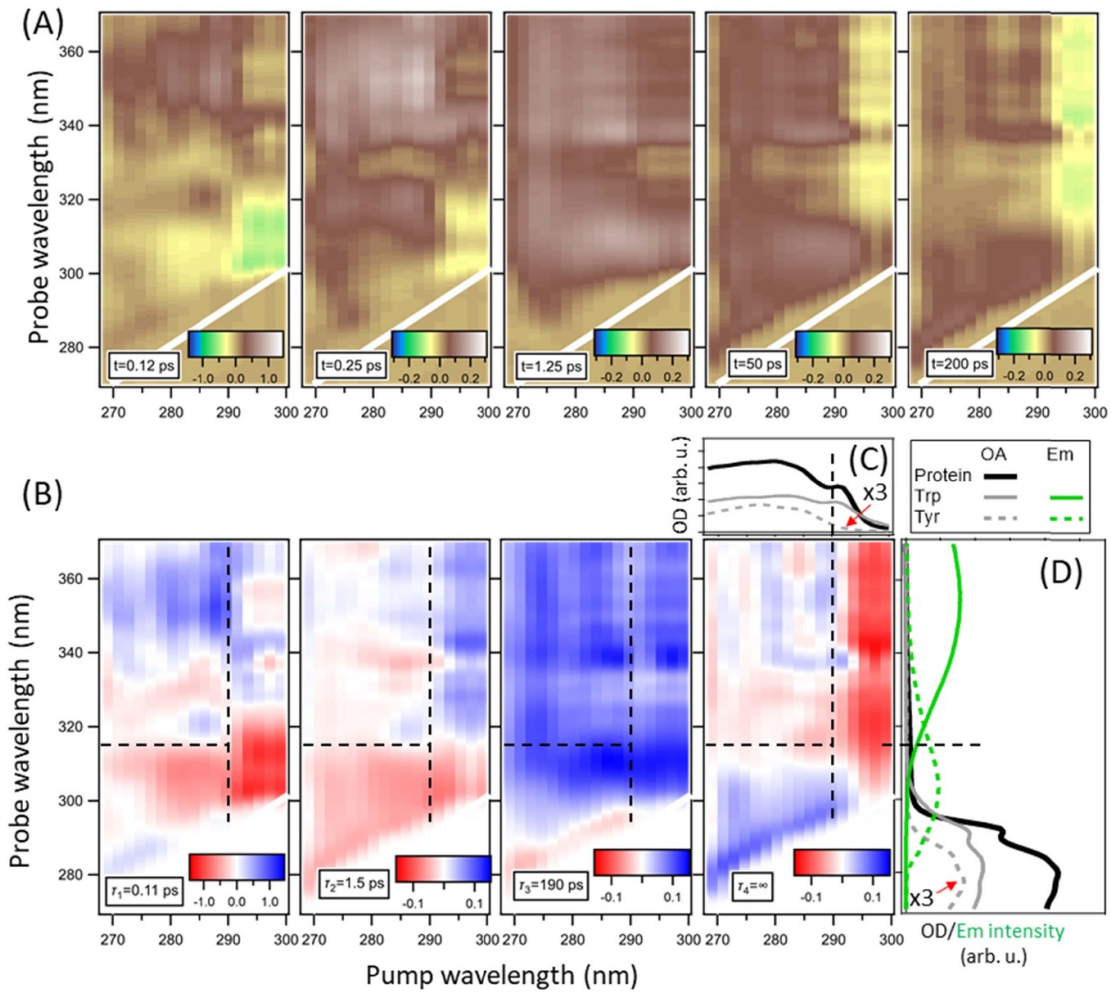

Figure 9. (A) a representative selection of 2D spectra of a wild-type P. aeruginosa azurin at physiological conditions at different times (0.12, 0.25, 1.25, 50, 200 ps). (B) DA2DSs, with the respective characteristic times, from a 3D SVD global analysis (section 2.5). (C) Steady-state absorption (OA) spectra of the protein (black solid line), tryptophan (Trp, grey solid line) and tyrosines (Tyr, grey dashed line). Since there are three tyrosines in the protein, the Tyr OA spectrum is multiplied by 3 (×3) to facilitate the comparison. (D) Same data as panel C along with the emission (Em) spectra of the isolated amino acids (solid and dashed lines for Trp and Tyr, respectively). The vertical and horizontal black dashed lines mark where the absorption and the emission bands, respectively, are dominated by the Trp or contain Tyr signals.

At a first visual inspection, we observe that all the DA2DSs, except the third one, show a distinct behaviour below and above $\lambda_{Pm} = 290$ nm (marked by the vertical dashed lines in figure 9(B)). This proves that the different excited states contributing to the total absorption band, do not relax into the same excited state but trigger different dynamics. Indeed, although this absorption band originates from a manifold of electronic transitions, if all the excited states would relax into the same electronic state, we should still observe the same dynamics regardless λ_{Pm}, except possibly in the earlier ps due to an initial different temperature of the chromophore. In the case of such a homogenous spectral response, each 2D plot and DA2DS should show the same spectrum along the probe dimension regardless the λ_{Pm}. Also, any photometrically corrected TAE spectrum should resemble, at least qualitatively, the steady state absorption band. Instead, we clearly observe that the signal not only does not follow the absorption spectrum but also changes sign. To explain the origin of the different behaviour below and above $\lambda_{Pm} = 290$ nm, it is convenient to compare the DA2DSs with the steady-state absorption spectra of Trp and Tyr (figure 9(C)). This reveals that the signals at $\lambda_{Pm} > 290$ nm are due to the excitation of Trp only, whereas the different behaviour observed at $\lambda_{Pm} < 290$ nm can be assigned to the excitation of Tyrs.

The examination of the fourth, $\tau = \infty$ DA2DS, which should mainly describe population dynamics (excited state decay and GSB recovery) without contributions from other ultrafast processes (as, for instance, vibrational redistribution, solvation, internal conversions, etc) confirms that the long-lasting negative signal at $\lambda_{Pm} > 290$ nm is the emission of Trp (see green solid line in figure 9(D)). This is indeed observed at $\lambda_{pr} > 315$ nm and is the only source of negative signals in this probe range. The excitation at $\lambda_{Pm} < 290$ nm

induces a positive ESA signal at any λ_{pr}, which competes with the negative stimulated emission (SE) signal from the Trp at $\lambda_{pr} > 315$ nm.

Remarkably only the third component shows the forenamed homogeneous behaviour, leading to the conclusion that it is due to either excited Tyr or exited Trp that initially relax to the same excited state. This is very likely the lowest excited state of the Trp, which can be directly excited at $\lambda > 290$ nm. In agreement with the long-lived emissive nature of this signal, we are inclined to interpret the $DA2DS_3$ as a rise of the SE, rather than a decay of an ESA signal. On the other hand, the TAE spectra at 350 nm, the maximum of the emission, at 50 ps and 200 ps are peaked around 280 nm resembling the Tyr absorption band (data not shown). Accordingly, this component should originate from an EnT from the excited Tyrs towards the Trp.

The first and second DA2DS are practically colour inverted with respect to $DA2DS_4$, which would drive us to the conclusion that they describe the relaxations bringing to the formation of the final state described by $DA2DS_4$, i.e. the rise of the Tyr ESA signals at $\lambda_{Pm} < 290$ nm and of the Trp SE at $\lambda_{Pm} > 290$ nm. However an alternative assignment is suggested by the comparison of $DA2DS_1$ and $DA2DS_2$ with the Tyr steady-state absorption and emission spectra (figure 9(C)), which are indeed all located at $\lambda < 320$ nm (the horizontal dashed line in figure 9(B) and D marks $\lambda_{pr} = 315$ nm). Accordingly, we expect to see only in this probe range the negative contributions stemming from GSB and SE of excited Tyrs, which can show only positive TA signals due to ESA at longer λ_{pr}. This is indeed the pattern observed in the first two DA2DSs and, considering that these dynamics are observed only at $\lambda_{Pm} < 290$ nm, we could assign the 2D signals at $\lambda_{Pm} < 290$ nm to the decay of excited tyrosines, On the other hand, the presence of the rise of negative signals at $\lambda_{pr} = 315$–370 nm (blue shaded areas) would point to a concomitant increase of Trp SE (the only source of negative signals in this region). This would suggest that, at least partially, one of the relaxation mechanisms of photoexcited Tyrs is an EnT towards the Trp.

The two interpretations move in opposite direction and further evidences and modelling are necessary to clarify the matter, but both lead to the conclusion that the Tyrs play a role in the first ps dynamics of the Trp transferring energy to the latter.

With due distinction, this is the same outcome from the analysis of $DA2DS_3$. The fact that we do not recognize a unique behaviour for the three Tyrs could simply be because each is characterized by its own set of energetics and geometrical parameters with respect to the Trp and the other Tyrs (distance, mutual orientation and couplings, local polarity, exposure to solvent, etc) reflecting in different dynamical behaviours.

This is only a preliminary interpretation that needs further discussion and modelling but, for the purposes of this article, clearly shows the richness of insights that a 2D study, even without sub-10 fs resolution, can give into the complex interplay between the Trp and the other aromatic amino acids of the protein, and in particular the three tyrosines (Tyr) present in the protein. It is worth noticing that can comfortably isolate the Tyr from Trp contributions mostly thanks to the capability to resolve the fine dependency of photometric TA signals on λ_{Pm}. In conclusion of this section it is worth commenting on sub-10 fs dynamics that we might have not resolved. Trp has two electronic transitions contributing to the UV absorption band, which originate from the two lowest exited electronic single states [2, 34, 36]. Since the one higher in energy relaxes into the low-lying state in less than 50 fs [36], we could expect some signature, if any, of this internal conversion in the earliest times and at most in the first DA2DS, which contains information on strong electronic and vibrational decoherence processes. The investigation of such dynamics would benefit from measurements with higher time-resolutions as FT-2D techniques.

4. Conclusion

Here we presented a noncoherent 2D spectrograph based on TA geometry with broad excitation (270–380 nm) and detection range (270–750 nm) and the capability to work with μl of sample volume. The combination of chirp mirrors for linear over compression of ultrabroad pulses, a reduction of the SHG crystal thickness and suppression of the compensation plate for beam walk-off, broadband shallow angle harmonic separators and the use of reflective optics only (except the 150 μm beam sampler for the photometric correction) results in the unprecedented temporal resolution of 33 fs (standard deviation). With a single-shot referenced detection, we achieve an SNR ratio of 10^5, or 10 μOD noise, per second of acquisition time. These methodological extensions in excitation and detection from UV to DUV is beyond the state of the art and make our implementation ideal to study transfer phenomena and long-range couplings in bio and biomimetic systems. We also extensively discussed how to extend advanced global data analysis techniques, usually conceived for 1D time-resolved techniques, to 2D data.

We exemplified the capabilities of our techniques by studying photo-induced excited state dynamics in a bio-inspired multi-chromophore antenna, made by stacked phenanthrenes, and intra-amino-acids couplings in an electron transfer Cu protein (a *P. aeruginosa* azurin). In the former case 2D spectroscopy allowed us to

observe and track down spectral diffusion of the ESA bands which speaks for a great degree of conformational disorder in the ground state. This reflects into an electronic or conformational heterogeneity of the photo-excited system but short lived. The details of such a transition is still unclear but it is striking that preliminary computational unpublished studies propose that the excited state relaxation are accompanied by a change in the rigidity of the stacking [37, 38]. Comparing TAE spectra with the steady-state absorption spectrum revealed the presence of a manifold of electronic transitions underneath the steady-states absorption band, each initiating a different photophysical response.

The latter scientific case represents a nice example of the richness of information that 2D spectroscopy with DUV detection can provide on the photophysics of a biomolecule. The capability of tracking down the fine dependency of photometric TA signals on the pump wavelength allows us isolating the Tyr from Trp contributions and disentangling the different dynamics by resolving their amplitudes, quantum yields and rates against λ_{Pm}. Our approach can give precious insights into the complex pattern of interactions between the Trp and the three Tyrs present in the protein. We definitively observe an involvement of the latter in the photophysics of the former. In agreement with the expectation that the Tyrs are not equivalent, we can identify different schemes of couplings.

Data availability statement

The data that support the findings of this study are available at the following URL/DOI: https://boris.unibe.ch/id/eprint/153520.

Acknowledgments

The investigation on the functional dynamics on the multi-chromophoric systems and the *P. aeruginosa* azurin have been carried out in tight collaboration with professor Robert Häner (University of Bern) and professor Antonín Vlček (J Heyrovský Institute of Physical Chemistry, Czech Academy of Sciences, and Queen Mary University of London), respectively. Authors are deeply grateful for their courtesy of letting us include unpublished data but even more for their availability, scientific discussion and support. Authors thank professor Antonio Monari (Université de Lorraine and CNRS) for his help in modelling the MCS photophysics with theoretical and computational methods. Authors acknowledge the support of Synertronic Designs, in the person of Timo Stehmann, in developing the Glaz LineScan platform according to the provided concept and specifications. AC, MN, AR acknowledge the financial support from the ERC Starting Grant 279599-FunctionalDyna and Swiss NSF through the NCCR MUST 'Molecular Ultrafast Science and Technology'. AC, MN and ACR are grateful to Swiss NSF via the project 200021_172696. AC thanks Professor Thomas Feurer (University of Bern) for the beautiful scientific discussions and relentless support.

ORCID iDs

Maryam Nazari Haghighi Pashaki https://orcid.org/0000-0002-0087-7334
Michela Gazzetto https://orcid.org/0000-0002-1968-7258
Andrea Cannizzo https://orcid.org/0000-0002-2325-0112

References

[1] Krebs N, Pugliesi I, Hauer J and Riedle E 2013 Two-dimensional Fourier transform spectroscopy in the ultraviolet with sub-20 fs pump pulses and 250–720 nm supercontinuum probe *New J. Phys.* **15** 85016
[2] Cannizzo A 2012 Ultrafast UV spectroscopy: from a local to a global view of dynamical processes in macromolecules *Phys. Chem. Chem. Phys.* **14** 11205–23
[3] Hamm P and Zanni M 2011 *Concepts and Methods of 2D Infrared Spectroscopy* (Cambridge: Cambridge University Press)
[4] Mukamel S 1995 *Principles of Nonlinear Optical Spectroscopy* (Oxford: Oxford University Press)
[5] Achazi G and Cannizzo A 2017 Fourier transform spectral interferometry with non-phase stable setups by broadband single shot detection of fs and ps pulses *Rev. Sci. Instrum.* **88** 83110
[6] Finkelstein I J, Zheng J, Ishikawa H, Kim S, Kwak K and Fayer M D 2007 Probing dynamics of complex molecular systems with ultrafast 2D IR vibrational echo spectroscopy *Phys. Chem. Chem. Phys.* **9** 1533–49
[7] Grumstrup E M, Shim S-H, Montgomery M A, Damrauer N H and Zanni M T 2007 Facile collection of two-dimensional electronic spectra using femtosecond pulse-shaping technology *Opt. Express* **15** 16681–9
[8] Bredenbeck J, Helbing J, Kolano C and Hamm P 2007 Ultrafast 2D-IR spectroscopy of transient species *ChemPhysChem* **8** 1747–56
[9] Brixner T, Mančal T, Stiopkin I V and Fleming G R 2004 Phase-stabilized two-dimensional electronic spectroscopy *J. Chem. Phys.* **121** 4221–36
[10] Auböck G, Consani C, Van Mourik F and Chergui M 2012 UV two-dimensional transient absorption spectroscopy *Res. Opt. Sci. OSA Tech. Dig. (Optical Soc. Am. 2012)* p IM3D.1
[11] Picchiotti A, Nenov A, Giussani A, Prokhorenko V I, Miller R J D, Mukamel S and Garavelli M 2019 Pyrene, a test case for deep-ultraviolet molecular photophysics *J. Phys. Chem. Lett.* **10** 3481–7

[12] Borrego-Varillas R, Nenov A, Ganzer L, Oriana A, Manzoni C, Tolomelli A, Rivalta I, Mukamel S, Garavelli M and Cerullo G 2019 Two-dimensional UV spectroscopy: a new insight into the structure and dynamics of biomolecules *Chem. Sci.* **10** 9907–21
[13] Song Y, Konar A, Sechrist R, Roy V P, Duan R, Dziurgot J, Policht V, Matutes Y A, Kubarych K J and Ogilvie J P 2019 Multispectral multidimensional spectrometer spanning the ultraviolet to the mid-infrared *Rev. Sci. Instrum.* **90** 13108
[14] Auböck G, Consani C, Van Mourik F and Chergui M 2012 Ultrabroadband femtosecond two-dimensional ultraviolet transient absorption *Opt. Lett.* **37** 2337–9
[15] Chergui M 2019 Ultrafast molecular photophysics in the deep-ultraviolet *J. Chem. Phys.* **150** 70901
[16] Son M, Mosquera-Vázquez S and Schlau-Cohen G S 2017 Ultrabroadband 2D electronic spectroscopy with high-speed, shot-to-shot detection *Opt. Express* **25** 18950–62
[17] Kearns N M, Jones A C, Kunz M B, Allen R T, Flach J T and Zanni M T 2019 Two-dimensional white-light spectroscopy using supercontinuum from an all-normal dispersion photonic crystal fiber pumped by a 70 MHz Yb fiber oscillator *J. Phys. Chem. A 2019* **123** 3046–55
[18] Bradler M, Baum P and Riedle E 2009 Femtosecond continuum generation in bulk laser host materials with sub-μJ pump pulses *Appl. Phys.* B **97** 561–74
[19] Záliš S, Consani C, Nahhas A E, Cannizzo A, Chergui M, Hartl F and Vlček A 2011 Origin of electronic absorption spectra of MLCT-excited and one-electron reduced 2,2′-bipyridine and 1, 10-phenanthroline complexes *Inorg. Chim. Acta* **374** 578–85
[20] Smith A V *SNLO Nonlinear Optics Code* (Albuquerque, NM: AS-Photonics)
[21] Chauvet A, Tibiletti T, Caffarri S and Chergui M 2014 A microfluidic flow-cell for the study of the ultrafast dynamics of biological systems *Rev. Sci. Instrum.* **85** 103118
[22] Slavov C, Hartmann H and Wachtveitl J 2015 Implementation and evaluation of data analysis strategies for time-resolved optical spectroscopy *Anal. Chem.* **87** 2328–36
[23] Ruckebusch C, Sliwa M, Pernot P, De Juan A and Tauler R 2012 Comprehensive data analysis of femtosecond transient absorption spectra : a review *J. Photochem. Photobiol.* C **13** 1–27
[24] Cannizzo A, Blanco-Rodríguez A M, El Nahhas A, Šebera J, Záliš S, Vlček A and Chergui M 2008 Femtosecond fluorescence and intersystem crossing in rhenium (I) carbonyl–bipyridine complexes *J. Am. Chem. Soc.* **130** 8967–74
[25] Nazari M *et al* 2019 Ultrafast dynamics in polycyclic aromatic hydrocarbons: the key case of conical intersections at higher excited states and their role in the photophysics of phenanthrene monomer *Phys. Chem. Chem. Phys.* **21** 16981–8
[26] Shih C *et al* 2008 Tryptophan-accelerated electron flow through proteins *Science* **320** 1760–2
[27] Consani C, Auböck G, Van Mourik F and Chergui M 2013 Ultrafast tryptophan-to-heme electron transfer in myoglobins revealed by UV 2D spectroscopy *Science.* **339** 1586–9
[28] Garo F 2012 Energy transfer in a DNA-based π-array on the use as light-harvesting antenna systems PhD Thesis University of Bern, Switzerland
[29] Garo F and Häner R 2012 A DNA-based light-harvesting antenna *Angew. Chem., Int. Ed.* **51** 916–9
[30] Langenegger S M 2005 Non-nucleosidic polyaromatic building blocks as DNA base surrogates PhD thesis University of Bern, Switzerland
[31] Probst M, Langenegger S M and Häner R 2014 A modular LHC built on the DNA three-way junction *Chem. Commun.* **50** 159–61
[32] Bösch C D *et al* 2019 DNA-organized light-harvesting antennae : energy transfer in polyaromatic stacks proceeds through interposed nucleobase pairs *Helv. Chim. Acta* **102** e1900148
[33] Winiger C B, Li S, Kumar G R, Langenegger S M and Häner R 2014 Long-distance electronic energy transfer in light-harvesting supramolecular polymers *Angew. Chem., Int. Ed.* **53** 13609–13
[34] Lakowicz J R 2006 *Principles of Fluorescence Spectroscopy* 3rd edn (Springer US) p 65
[35] Blanco-Rodríguez A M *et al* 2011 Phototriggering electron flow through Re^{I}-modified Pseudomonas aeruginosa azurins *Chem. Eur. J.* **17** 5350–61
[36] Braem O, Penfold T J, Cannizzo A and Chergui M 2012 A femtosecond fluorescence study of vibrational relaxation and cooling dynamics of UV dyes *Phys. Chem. Chem. Phys.* **14** 3513–9
[37] Monari A Private communication
[38] Blanc A 2020 Etude théorique des phénomènes de transport cohérent d'énergie et de charge dans les systèmes auto-organiseś et de la propagation des excitons (Theoretical study of coherent energy and charge transport phenomena in self-assembled systems and of exciton exciton propagation) Université de Lorraine- Nancy, France Supervisor Professor Antonio Monari